Microscopic Picture of Erosion and Sedimentation Processes in Dense Granular Flows

Denis Dumont,[1] Pierre Soulard,[2] Thomas Salez,[3,4] Elie Raphaël,[2,*] and Pascal Damman[1,†]
[1]Laboratoire Interfaces et Fluides Complexes, Université de Mons, 20 Place du Parc, B-7000 Mons, Belgium
[2]UMR CNRS Gulliver 7083, ESPCI Paris, PSL Research University, 75005 Paris, France
[3]Univ. Bordeaux, CNRS, LOMA, UMR 5798, F-33405 Talence, France
[4]Global Station for Soft Matter, Global Institution for Collaborative Research and Education, Hokkaido University, 060-0808 Sapporo, Japan

(Received 6 January 2020; revised 28 May 2020; accepted 29 September 2020; published 10 November 2020)

Gravity-driven flows of granular matter are involved in a wide variety of situations, ranging from industrial processes to geophysical phenomena, such as avalanches or landslides. These flows are characterized by the coexistence of solid and fluid phases, whose stability is directly related to the erosion and sedimentation occurring at the solid-fluid interface. To describe these mechanisms, we build a microscopic model involving friction, geometry, and a nonlocal cooperativity emerging from the propagation of collisions. This new picture enables us to obtain a detailed description of the exchanges between the fluid and solid phases. The model predicts a phase diagram including the limits of erosion and sedimentation, in quantitative agreement with experiments and discrete-element-method simulations.

DOI: 10.1103/PhysRevLett.125.208002

Over the last two decades, different theoretical approaches have been proposed to describe dense granular flows. The most widely used models are based on the $\mu(I)$ rheology [1]. This approach consists of a semiempirical description of granular matter, through an effective friction coefficient μ, that is a function of an inertial number I directly related to the flow velocity [2]. Extensions of this $\mu(I)$ rheology have been proposed by several authors to address spatial heterogeneities and nonlocal effects [3–7]. For instance, the yield stress increases as the thickness of the flow region reduces, which manifests itself through a thickness-dependent stop angle in granular flows down inclined planes [8]. In parallel, semiempirical models have been developed to describe the dynamics of dense granular flows atop static granular solids. These systems exhibit complex behaviors due to the transfers of energy and matter between the fluid and solid phases at their interface. The erosion of the solid phase by an avalanche feeds the fluid phase, whereas the sedimentation of the fluid phase tends to stop the motion. The Bouchaud-Cates-Ravi-Prakash-Edwards (BCRE) model was proposed to account for this coupled dynamics [9–12]. The two key ingredients of this approach are (i) the intuitive idea that the evolution of the interface between the two phases is determined by its local tilt angle θ (see Fig. 1); and (ii) the assumed existence of a neutral angle θ^* such that for $\theta > \theta^*$, erosion occurs, whereas for $\theta < \theta^*$, sedimentation occurs. Subsequent studies suggested that $\theta^* = \arctan(\mu_{\rm dyn})$ [13], where $\mu_{\rm dyn}$ is an effective friction coefficient depending on the flow rate and the fluid-layer thickness [14].

In this Letter, we propose a new microscopic description of the erosion and sedimentation processes at play in dense granular flows driven by gravity. Our model involves a flowing layer of grains over a static, yet erodible one and includes a nonlocal cooperativity emerging from the propagation of collisions. Its predictions are directly confronted to numerical results obtained from discrete-element-method (DEM) simulations in two canonical configurations: an inclined plane and a heap. Despite its simplicity, the proposed model enables us to obtain a detailed description of the exchange mechanisms between the fluid and solid phases, as well as a complete phase diagram of erosion and sedimentation. The model quantitatively describes the observed transitions between sedimentation, stationary flow, and erosion. Moreover, it allows us to rationalize an important observable from inclined-plane experiments in the literature: the stop angle of a granular flow.

We consider a system made of spheres of diameter d and mass m, with an interparticle sliding (resp rolling) friction coefficient μ_S (resp μ_R) [15]. These two coefficients are merged into a single effective coefficient $\mu_{\rm eff}$ [16]. Our description is a mean field approach, involving average quantities and avoiding the actual irregularities present in a real granular medium. As schematized in Fig. 1, we consider a moving layer of thickness $\mathcal{R}$ (in number of grains and counted vertically), i.e., the fluid phase, above a static layer, i.e., the solid phase. The roughness of the solid-fluid interface is characterized by an angle $\varphi_{\rm sol}$ with respect to the normal to the interface, quantifying the angular depth of the hole between two grains. The value of $\varphi_{\rm sol}$ ranges between 23.4° and 30° for spherical grains [23]. In the following, we focus on the motion of a single moving grain at the solid-fluid interface. This grain is subjected to the weight exerted by the $\mathcal{R}$ grains above it, belonging to the

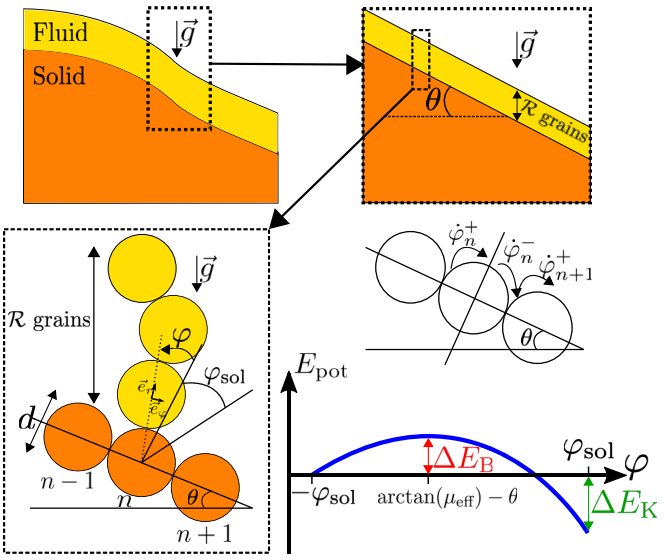

FIG. 1. A dense fluid phase (yellow) moves over a static solid phase (orange). The instantaneous position of a grain, moving above a static grain n, is described through the angle φ (see text for details). Also shown is the effective potential energy $E_{\rm pot}(\varphi)$, during the first step of the grain motion, within one cycle where $\varphi \in [-\varphi_{\rm sol}, +\varphi_{\rm sol}]$.

moving layer and is not allowed to jump. To move forward, the grain has to slide and/or roll over the bumpy underlying static layer. The instantaneous position of the moving grain is described through a single variable: the angle φ between the normal to the interface and the contact interparticle-distance unit vector $\vec{e}_r$ (see Fig. 1).

As in previous studies [24–26], the motion is divided into two subsequent steps. First, the grain starts at angular position $-\varphi_{\rm sol}$ with angular velocity $\dot{\varphi}_n^+$, and then it moves above a static grain indexed by n until it arrives at $+\varphi_{\rm sol}$ with angular velocity $\dot{\varphi}_n^-$. Second, it elastically collides with the next static grain indexed by $n+1$, which induces a sharp change of its velocity (orientation and norm), as well as secondary elastic collisions within the fluid and solid phases. A new cycle then starts for the moving grain, with an initial angular velocity $\dot{\varphi}_{n+1}^+$.

During the first step, the trajectory of the grain is circular. The force components that contribute to the variation of its kinetic energy are along the tangential unit vector $\vec{e}_\varphi$: the transverse projection $\mathcal{R}mg\sin(\varphi+\theta)\vec{e}_\varphi$ of the weight, and the effective friction force $-\mu_{\rm eff}\mathcal{R}mg\cos(\varphi+\theta)\vec{e}_\varphi$ generated by the normal projection of the weight. We assumed that most of the frictional dissipation occurs through the contact of the moving grain and the static layer, since all the grains of the moving layer have similar velocities.

The total force along $\vec{e}_\varphi$ can be recast as the derivative of an effective potential energy, $-(1/d)dE_{\rm pot}/d\varphi$, where

$$E_{\rm pot}(\varphi) = \mathcal{R}mgd\{\cos(\varphi+\theta) - \cos(\varphi_{\rm sol}-\theta) + \mu_{\rm eff}[\sin(\varphi+\theta) + \sin(\varphi_{\rm sol}-\theta)]\}.$$

The origin of energies has been chosen at $\varphi = -\varphi_{\rm sol}$ (see Fig. 1). At $\varphi = \arctan(\mu_{\rm eff}) - \theta$, this potential energy is maximal, resulting in an energy barrier that the grain has to overcome:

$$\Delta E_B = \mathcal{R}mgd\left[\sqrt{1+\mu_{\rm eff}^2} - \cos(\varphi_{\rm sol}-\theta) + \mu_{\rm eff}\sin(\varphi_{\rm sol}-\theta)\right]. \quad (1)$$

If the moving grain has enough initial kinetic energy $md^2(\dot{\varphi}_n^+)^2/2$ to overcome the barrier, it gains at the end of the first step the kinetic energy:

$$\Delta E_K = \frac{md^2}{2}[(\dot{\varphi}_n^-)^2 - (\dot{\varphi}_n^+)^2], \quad (2)$$

$$= 2\mathcal{R}mgd[\sin(\theta) - \mu_{\rm eff}\cos(\theta)]\sin(\varphi_{\rm sol}). \quad (3)$$

Up to now, we have not considered the contacts between grains within each of the two layers, leading to the nonlocal cooperative effects. In our model, these naturally appear in the second step of motion. Indeed, after the primary elastic collision with the $(n+1)$th static grain (see Fig. 1), the velocity of the considered moving grain changes suddenly; and cascades of secondary elastic collisions occur within the fluid and solid phases. This process leads to a cooperative energy reallocation that forms the essence of nonlocality. The energy transferred by the moving grain to the static grain during the primary collision is assumed to be proportional to the incoming energy, and it reads $amd^2(\dot{\varphi}_n^-)^2/2$, with a a constant prefactor $(0 < a < 1)$. After the primary collision, the energies of the moving grain and the static grain temporarily become $(1-a)md^2(\dot{\varphi}_n^-)^2/2$ and $amd^2(\dot{\varphi}_n^-)^2/2$ before energy reallocation. Then, cascades of secondary elastic collisions are triggered in both phases. In a minimal description, we assume that they involve (i) $\mathcal{N}_{\rm flu}$ and $\mathcal{N}_{\rm sol}$ grains in the fluid and solid phases; and (ii) some energy equipartition among those grains.

For the fluid phase, the energy primarily lost by the moving grain is redistributed over the $\mathcal{N}_{\rm flu}$ moving grains. Over the primary and secondary collisions, the total energy loss $\Delta E_0 = md^2[(\dot{\varphi}_n^-)^2 - (\dot{\varphi}_{n+1}^+)^2]/2$ for the moving grain thus reads

$$\Delta E_0 = \frac{amd^2}{2\mathcal{N}_{\rm flu}}(\dot{\varphi}_n^-)^2. \quad (4)$$

As a consequence, the ratio $\alpha = (\dot{\varphi}_{n+1}^+/\dot{\varphi}_n^-)^2$ between the kinetic energies after and before the collisions is given by $\alpha = 1 - a/\mathcal{N}_{\rm flu}$ and represents a direct signature of cooperativity in the fluid phase. Invoking the previous relations and Eq. (2), one finally gets the central recursive equation

$$(\dot{\varphi}^{+}_{n+1})^2 = \alpha\left[(\dot{\varphi}^{+}_{n})^2 + \frac{2\Delta E_K}{md^2}\right]. \quad (5)$$

Assuming a global translational invariance in the system, and thus looking for the fixed point of Eq. (5), one gets $(\dot{\varphi}^{+}_{\infty})^2 = 2\alpha\Delta E_K/[md^2(1-\alpha)]$. In this homogeneous state, during each cycle, the kinetic energy gained by the moving grain when going down the effective potential is exactly compensated for by the loss due to the subsequent collisional process, such that $\Delta E_K = \Delta E_0$. The homogeneous state is stable only if the associated kinetic energy $E_K^{\infty} = md^2(\dot{\varphi}^{+}_{\infty})^2/2 = \alpha\Delta E_K/(1-\alpha)$, set by Eq. (3), is larger than the barrier ΔE_B, set by Eq. (1), giving a limiting condition

$$\frac{\alpha}{1-\alpha}\Delta E_K(\theta_{\rm sed}, \mathcal{R}) = \Delta E_B(\theta_{\rm sed}, \mathcal{R}), \quad (6)$$

which determines the sedimentation angle $\theta_{\rm sed}(\mathcal{R})$. If $\theta < \theta_{\rm sed}$, the lowest layer of the fluid phase stops, and $\mathcal{R}$ decreases. If $\theta > \theta_{\rm sed}$, the kinetic energy is higher than the potential barrier, and the lowest layer of the fluid phase does not stop.

A similar reasoning allows us to discuss erosion. Considering the solid phase, the energy $amd^2(\dot{\varphi}^{-}_{n})^2/2$ gained by the static grain at the solid-fluid interface after the primary collision is redistributed over the $\mathcal{N}_{\rm sol}$ static grains through the cascade of secondary elastic collisions. Over one complete cycle, the solid phase receives a global energy $amd^2(\dot{\varphi}^{-}_{\infty})^2/2 = \mathcal{N}_{\rm flu}\Delta E_K$. Invoking the energy equipartition among the $\mathcal{N}_{\rm sol}$ grains, the static grain at the solid-fluid interface thus receives an overall net kinetic energy $\mathcal{N}_{\rm flu}\Delta E_K/\mathcal{N}_{\rm sol}$, set by Eq. (3). The homogeneous state is stable only if this kinetic energy remains smaller than the energy required to drive the static grain into motion, given by the energy barrier $\Delta E_B(\theta, \mathcal{R}+1)$, set by Eq. (1). The limiting condition

$$\frac{\mathcal{N}_{\rm flu}}{\mathcal{N}_{\rm sol}}\Delta E_K(\theta_{\rm ero}, \mathcal{R}) = \Delta E_B(\theta_{\rm ero}, \mathcal{R}+1) \quad (7)$$

determines the erosion angle $\theta_{\rm ero}(\mathcal{R})$. If $\theta > \theta_{\rm ero}$, the highest layer of the solid phase starts to flow, and $\mathcal{R}$ increases. The right-hand side of Eq. (7) represents the absolute value of a cohesion energy of the solid phase. For dry granular assembly, only friction and geometry control this cohesion. However, additional forces can be added in Eq. (7), such as capillary forces for wet grains [2,27]. The static grains can even be glued, as in inclined-plane experiments [8].

To solve Eqs. (6) and (7), we need to specify further $\mathcal{N}_{\rm sol}$ and $\mathcal{N}_{\rm flu}$, i.e., the shape and size of the cooperative regions in each phase. In the bulk, we assume a cooperative region of either phase to contain ξ grains and to have a fractal dimension D. Its typical length scale is given by $\sim\xi^{1/D}$. When the thickness of a phase becomes smaller than $\xi^{1/D}$, the cooperative regions are altered by the boundaries and the bulk description should be modified. In a heap-flow configuration, the solid phase is deep enough to ensure that $\mathcal{N}_{\rm sol} = \xi$. In contrast, the fluid-air interface acts as a free-volume reservoir, which is expected to truncate the neighboring cooperative regions. At small $\mathcal{R}/\xi^{1/D}$, the number of grains in the cooperative regions of the fluid phase becomes $\sim\xi^{1-1/D}\mathcal{R}$, whereas at large $\mathcal{R}/\xi^{1/D}$, it saturates to ξ. To interpolate these two limiting behaviors, we propose the ansatz $\mathcal{N}_{\rm flu}(\mathcal{R}) = \xi[1-\exp(-\mathcal{R}/\xi^{1/D})]$. It should be noted that the precise functional form defining $\mathcal{N}_{\rm flu}(\mathcal{R})$ is not crucial because other expressions produce similar results [16]. The key point here is that $\mathcal{N}_{\rm flu}$ first increases with $\mathcal{R}$ before saturating.

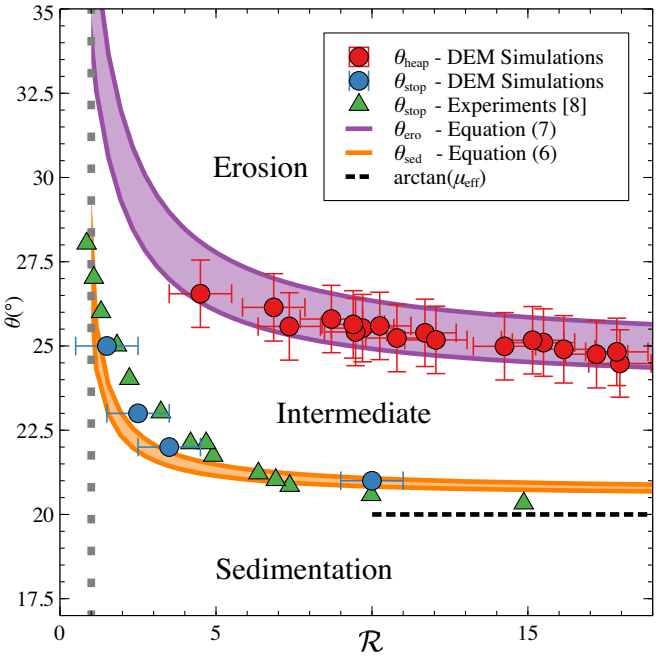

FIG. 2. The $\theta - \mathcal{R}$ phase diagram. Results from (i) DEM simulations for inclined-plane ($\theta_{\rm stop}$) and heap ($\theta_{\rm heap}$) configurations; (ii) inclined-plane experiments ($\theta_{\rm stop}$) [8]; and (iii) predictions ($\theta_{\rm ero}$, $\theta_{\rm sed}$) from the model. The fixed parameters are $\mu_{\rm eff} = \tan(20°)$ [8], $a = 0.5$ [24], and $\varphi_{\rm sol} \in [23.4°, 30°]$ [23]. The two adjustable parameters are $\xi = 4.7$ and $D = 0.94$. The horizontal and vertical dashed lines indicate $\theta = \arctan(\mu_{\rm eff})$ and $\mathcal{R} = 1$.

With these expressions for $\mathcal{N}_{\rm sol}$ and $\mathcal{N}_{\rm flu}$, the evolutions of $\theta_{\rm sed}$ and $\theta_{\rm ero}$ can be computed by numerically solving Eqs. (6) and (7). There are five dimensionless parameters: $\mu_{\rm eff}$, $\varphi_{\rm sol}$, a, ξ, and D. The coefficient a is close to 0.5 [24], whereas the effective friction coefficient is fixed to $\mu_{\rm eff} = \tan(20°)$ [16] and $\varphi_{\rm sol}$ spans the range [23.4°,30°] [23]. Thus, ξ and D are the only free parameters. As shown in Fig. 2, $\theta_{\rm sed}$ and $\theta_{\rm ero}$ rapidly decrease as $\mathcal{R}$ increases over a typical length scale $\sim\xi^{1/D}$ before saturating for thick fluid phases. For large $\mathcal{R}$, the sedimentation angle is close to $\arctan(\mu_{\rm eff})$, whereas the erosion angle is clearly above.

These two curves define sedimentation and erosion, and they collectively determine the phase diagram for a flowing layer of grains atop a static one. Below the $\theta_{\mathrm{sed}}(\mathcal{R})$ curve, the flow is unstable. The moving grains at the solid-fluid interface do not have enough kinetic energy to overcome their potential barrier (see Fig. 1). Therefore, the thickness of the fluid phase decreases continuously and full sedimentation eventually occurs. Above the $\theta_{\mathrm{ero}}(\mathcal{R})$ curve, the energy transmitted from the fluid phase to the solid one through collisions is sufficient for the barrier energy of the static grains at the solid-fluid interface to be overcome. The thickness of the fluid phase increases continuously, and full erosion eventually occurs. In between these curves, the model predicts neither sedimentation nor erosion, and the flow might be considered as stable.

To test the model, one should ideally investigate the flow stability for experiments or numerical simulations with various $(\theta, \mathcal{R})$ sampling the three domains of the phase diagram. For practical reasons, it is difficult to design such tests. Finite-size heap-flow experiments involve a continuous injection of grains at the top and their removal at the bottom. The fluid-phase thickness $\mathcal{R}(Q)$ and heap angle $\theta_{\mathrm{heap}}(Q)$ self-adjust to the incoming flux Q of grains until a stationary state is reached—they cannot be controlled independently. In practice, we only have access to a unique relation $\theta_{\mathrm{heap}}(\mathcal{R})$. Nevertheless, by building the initial heap with a sufficiently large angle (e.g., near 90°), we enforce the system to start far up in the erosion domain. Subsequently, erosion occurs until the θ_{ero} line is reached. The heap spontaneously stabilizes at the upper limit of the stationary zone, thus allowing for a practical determination of $\theta_{\mathrm{ero}}(\mathcal{R})$.

In order to probe the sedimentation limit, the inclined-plane configuration [8,28–31] is particularly relevant. The solid phase is made of a nonerodible monolayer of grains glued on the incline [i.e., right-hand side of Eq. (7) becomes infinite]. The central observable is the stop angle θ_{stop}, defined as the minimal tilt angle of the substrate for which a stationary flow is observed. As discussed above, when $\theta < \theta_{\mathrm{sed}}(\mathcal{R})$, the lowest layer of the fluid phase stops and $\mathcal{R}$ reduces by one unit. As shown in Fig. 2, the monotonic decrease of $\theta_{\mathrm{sed}}(\mathcal{R})$ suggests that the system remains in the sedimentation domain. The sedimentation front thus propagates upwards in the granular assembly, until the whole system is stopped. The stop angle should be identified to the sedimentation one, thus allowing for a practical determination of $\theta_{\mathrm{sed}}(\mathcal{R})$.

We performed DEM numerical simulations for these two experimental configurations: heap and inclined plane (see Fig. 3) with the same microscopic parameters [16]. As shown in Fig. 2, the DEM results for the two different configurations and previous experimental results for the inclined-plane configuration [8] are in quantitative agreement with the model predictions under the proposed identifications: $\theta_{\mathrm{heap}} \simeq \theta_{\mathrm{ero}}$ and $\theta_{\mathrm{stop}} \simeq \theta_{\mathrm{sed}}$. The best-fit values of the two free parameters are $D = 0.94$ and

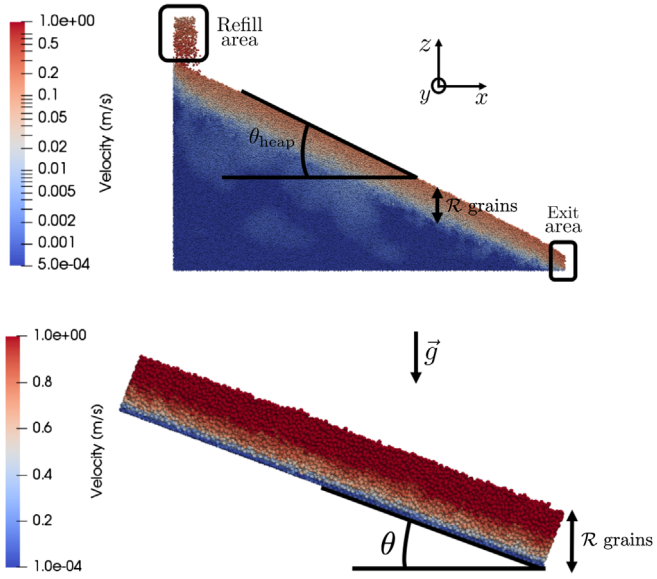

FIG. 3. Snapshots of the DEM simulations for (top) heap flow with fixed flow rate and (bottom) inclined-plane flow. The color maps refer to the velocity of the grains, as indicated in the scale bar.

$\xi = 4.7$, which suggest chainlike cooperative regions of a few grains and might be related to the force-chain network in static granular contact [32,33]. The two limiting $\theta(\mathcal{R})$ curves emerging from the model are corroborated by experiments and/or simulations. Above θ_{ero}, there is necessarily erosion; and below θ_{sed}, there is perforce sedimentation. To probe the intermediate region, we carried out additional simulations. In the inclined-plane configuration, we enforce the system to start in a biphasic composition, i.e., a flowing layer of grains atop a static one made of frozen grains [16]. After equilibration, we release all the grains of the static layer at once. With the parameters used here, we observe that the flowing grains fully erode the static layer to ultimately yield a single flowing layer. Malloggi *et al.* performed experiments for similar systems [30]. They observed that the final stationary state depends on the nature of the grains. The static layer is stable for sand while full erosion is observed for glass beads. In between the erosion and sedimentation limits, while our mean-field model is consistent with stable flow, experimental observations show that either erosion, sedimentation, or stable flow might occur, depending on the experimental conditions (nature of grains, boundary conditions). The intermediate region is quite sensitive to fluctuations, and it might not be described by a mean-field model. Further refinements should then include fluctuations, dilatancy, and other processes. Nevertheless, our results suggest that below θ_{sed} and above θ_{ero}, the fluctuations are negligible and the mean-field description is relevant.

Since $\theta_{\mathrm{sed}}(\mathcal{R}) < \theta_{\mathrm{ero}}(\mathcal{R})$, stationary flows might exist for angles ranging between these two disjoined boundaries. First, this opens a gap within the BCRE picture [10],

characterized by a single neutral angle θ^*: within our description, this neutral angle should be split into two distinct angles. Second, the decays of θ_{sed} and θ_{ero} with $\mathcal{R}$ are direct consequences of the energy-equipartition and cooperativity-truncation ingredients in the model. An increase of $\mathcal{R}$ implies that more grains of the fluid phase share the energy losses due to the collisions with the static layer, which renders flow and erosion easier, i.e., requiring smaller angles. Surface flow in yielded athermal granular media are inhibited by the truncation of cooperativity—as opposed to supercooled liquids at equilibrium [34]. Third, the saturations of $\theta_{\mathrm{sed}}(\mathcal{R})$ and $\theta_{\mathrm{ero}}(\mathcal{R})$ at large $\mathcal{R}$ are consistent with observations showing that the flow properties of thick granular layers are independent of the fluid-phase thickness [2,8]. This allows us to reconsider the previous suggestion of a friction coefficient depending on the fluid-layer thickness $\mathcal{R}$ [13,14].

In conclusion, we built a novel microscopic model involving friction, geometry, and nonlocal collisional effects to describe erosion and sedimentation processes in dense granular flows atop static granular layers. In contrast to previous work [9–11], our model suggests that each process might have its own critical angle, which depends on the fluid-layer thickness. This indicates the existence of an intermediate region, between these two limits, where granular systems become quite sensitive to experimental details, which would probably require beyond-mean-field refinements. Besides, the increase of both the erosion and sedimentation angles as the fluid-layer thickness decreases could be rationalized by considering a reduction in size of the cooperative region in the fluid phase. From our model, two classical experimental configurations—inclined plane and heap—(usually analyzed separately) could be described within a unified picture through a single phase diagram. These results might be useful in the design of hydrodynamic models, such as BCRE and the depth-averaged method [35].

This work benefited from financial support by the Fonds National de la Recherche Scientifique (FNRS; PDR research Project No. T.0109.16 "Capture Biomimétique de Fluide" and CDR Project No. J.0191.17 "Mimicking Elasticity with Viscous Fluids"), and by the Action de Recherche Concertée (UMONS, research project "Mecafood"). D. D. acknowledges funding from FNRS through the Foundation for Training in Industrial and Agricultural Research. The authors also thank Yacine Amarouchene, Fabian Brau, and Paul Rambach for fruitful discussions.

D. D. and P. S. contributed equally to this work.

*elie.raphael@espci.fr
†pascal.damman@umons.ac.be

[1] P. Jop, Y. Forterre, and O. Pouliquen, Nature (London) **441**, 727 (2006).
[2] B. Andreotti, Y. Forterre, and O. Pouliquen, *Granular Media: Between Fluid and Solid* (Cambridge University Press, Cambridge, England, 2013).
[3] O. Pouliquen and Y. Forterre, Phil. Trans. R. Soc. A **367**, 5091 (2009).
[4] K. Kamrin and G. Koval, Phys. Rev. Lett. **108**, 178301 (2012).
[5] M. Bouzid, M. Trulsson, P. Claudin, E. Clément, and B. Andreotti, Phys. Rev. Lett. **111**, 238301 (2013).
[6] M. Bouzid, A. Izzet, M. Trulsson, E. Clément, P. Claudin, and B. Andreotti, Eur. Phys. J. E **38**, 125 (2015).
[7] K. Kamrin, Front. Phys. **7**, 116 (2019).
[8] O. Pouliquen, Phys. Fluids **11**, 542 (1999).
[9] J.-P. Bouchaud, M. E. Cates, J. Ravi Prakash, and S. F. Edwards, J. Phys. I (France) **4**, 1383 (1994).
[10] J. P. Bouchaud, M. E. Cates, J. R. Prakash, and S. F. Edwards, Phys. Rev. Lett. **74**, 1982 (1995).
[11] T. Boutreux, E. Raphaël, and P. G. de Gennes, Phys. Rev. E **58**, 4692 (1998).
[12] T. Trinh, P. Boltenhagen, R. Delannay, and A. Valance, Phys. Rev. E **96**, 042904 (2017).
[13] A. Aradian, E. Raphaël, and P. G. de Gennes, C.R. Phys. **3**, 187 (2002).
[14] S. Douady, B. Andreotti, and A. Daerr, Eur. Phys. J. B **11**, 131 (1999).
[15] N. Estrada, E Azema, F. Radjai, and A. Taboada, Phys. Rev. E **84**, 011306 (2011).
[16] See Supplemental Material at http://link.aps.org/supplemental/10.1103/PhysRevLett.125.208002 for a discussion about friction coefficients and a detailed description of the DEM simulations, which include Refs. [17–22].
[17] C. Kloss, C. Goniva, A. Hager, S. Amberger, and S. Pirker, Prog. Comput. Fluid Dyn. **12**, 140 (2012).
[18] LIGGGHTS(R)-PUBLIC Documentation, Version 3.X, DCS Computing GmbH, JKU Linz and Sandia Corporation (2016), https://www.cfdem.com/media/DEM/docu/gran_model_hertz.html.
[19] P. Jop, Y. Forterre, and O. Pouliquen, J. Fluid Mech. **541**, 167 (2005).
[20] A. V. Orpe and D. V. Khakhar, Phys. Rev. Lett. **93**, 068001 (2004).
[21] A. V. Orpe and D. V. Khakhar, J. Fluid Mech. **571**, 1 (2007).
[22] P. A. Lemieux and D. J. Durian, Phys. Rev. Lett. **85**, 4273 (2000).
[23] R. Albert, I. Albert, D. Hornbaker, P. Schiffer, and A. L. Barabási, Phys. Rev. E **56**, R6271 (1997).
[24] L. Quartier, B. Andreotti, S. Douady, and A. Daerr, Phys. Rev. E **62**, 8299 (2000).
[25] B. Andreotti and S. Douady, Phys. Rev. E **63**, 031305 (2001).
[26] B. Andreotti, Europhys. Lett. **79**, 34001 (2007).
[27] G. Saingier, A. Sauret, and P. Jop, Phys. Rev. Lett. **118**, 208001 (2017).
[28] L. E. Silbert, D. Ertas, G. S. Grest, T. C. Halsey, D. Levine, and S. J. Plimpton, Phys. Rev. E **64**, 051302 (2001).
[29] T. Borzsonyi, T. C. Halsey, and R. E. Ecke, Phys. Rev. E **78**, 011306 (2008).
[30] F. Malloggi, B. Andreotti, and E. Clément, Phys. Rev. E **91**, 052202 (2015).
[31] K. Kamrin and D. L. Henann, Soft Matter **11**, 179 (2015).

[32] J. Geng, D. Howell, E. Longhi, R. P. Behringer, G. Reydellet, L. Vanel, E. Clément, and S. Luding, Phys. Rev. Lett. **87**, 035506 (2001).

[33] T. Majmudar and R. Behringer, Nature (London) **435**, 1079 (2005).

[34] T. Salez, J. Salez, K. Dalnoki-Veress, E. Raphaël, and J. A. Forrest, Proc. Natl. Acad. Sci. U.S.A. **112**, 8227 (2015).

[35] A. N. Edwards and J. M. N. T. Gray, J. Fluid Mech. **762**, 35 (2015).